Department of Ocean and Resources Engineering
School of Ocean and Earth Science and Technology

UNIVERSITY of HAWAI'I MĀNOA

January 16, 2018

Leo Rustum J. Espia
Deputy Administrator and State Hazard Mitigation Officer
Guam Homeland Security and Office of Civil Defense
221-B Chalan Palasyo, Agana Heights
Guam 96910

RE: Progress Report "Tsunami Safety Products for Apra Harbor, Guam"

Dear Mr. Espia,

Attached please find the above referenced report that summaries the background, methodology, and data products for Apra Harbor. This submittal also includes a set of hazard maps in ArcGIS format. If you need additional information, please contact me by phone at (808) 956-3485 or by email at cheung@hawaii.edu.

Yours truly,

Kwok Fai Cheung, PhD, PE
Professor and Graduate Chair

2450 Dole Street, Holmes 402, Honolulu, Hawai'i 96822
Telephone: 808.956.7572 Fax: 808.956.3498

Background

The National Tsunami Hazard Mitigation Program (NTHMP) is supporting state and regional efforts in developing tsunami safety products for the maritime communities. Guam Homeland Security began the modeling and mapping effort with the University of Hawaii in November 2017. Stakeholder meetings with United States Coast Guard (USCG) District 14 Sector Guam, Port Authority of Guam, Guam Naval Base Emergency Management, Guam Waterworks Authority, and Guam Power Authority provided guidance in defining the data products. The USCG District 14 operating procedures call for evacuation of ships and shore personnel in a tsunami warning, when the predicted nearshore wave amplitude is over 1 m, but do not have provisions for tsunami advisories, which involve predicted near-shore amplitude of less than 1 m. Localized currents and drawdown might pose navigational hazards and damage ships and mooring systems in spite of low potential for inundation. In support of emergency responses to warnings and advisories, the data products include offshore surge and current based on probable maximum tsunami scenarios as well as in-harbor hazard maps of surge, drawdown, and current for hypothetical advisory-level tsunamis from potential source regions. This progress report summarizes the tsunami scenarios, modeling procedures, and data products for Apra Harbor.

1. Tsunami Scenarios

A sensitivity analysis helps identify tsunami sources most critical to Guam for data product development. Gica et al. (2008) discretized the subduction zones of the Pacific into subfaults and compiled the fault parameters that can be implemented in the planar fault model of Okada (1985) to determine the seafloor deformation in earthquake rupture. We utilize NEOWAVE (Non-hydrostatic Evolution of Ocean Waves) to model the tsunamis from hypothetical *Mw* 8.5 earthquakes at the individual subfaults. Figure 1 shows the computed wave amplitude at 500 m water depth outside Apra Harbor from the respective sources. The results indicate the Mariana, Nankai, Ryukyu, Philippine, New Guinea, and Manus subduction zones are potentially critical to Guam. Tsunamis from the New Britain, Solomon, and New Hebrides subduction zones, Tonga-Kermadec Trench, and the Americas in general have relatively minor effects. The wave amplitude from sources at the westernmost Aleutians is appreciable, but is probably overestimated as the relative plate motion is approaching trench parallel toward Kamchatka (Lay et al., 2017).

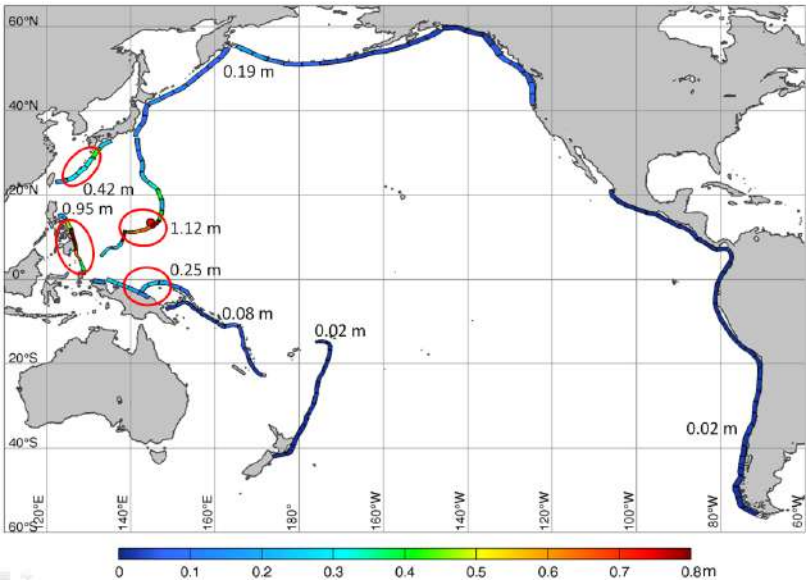

Figure 1. Sensitivity analysis of tsunami wave amplitude outside Apra Harbor from hypothetical *Mw* 8.5 earthquakes at subduction zones in the Pacific Ocean.

Table 1 summarizes the dip angles of the tsunami sources around Guam from Gica et al. (2008) and the convergence rate, coupling coefficient, and maximum magnitude from the Global Earthquake Model of Berryman et al. (2015). The potential tsunami threats can be categorized by the source location or approaching direction. The Mariana subduction zone is nearest to Guam and a tsunami generated there has little time for warning and response. Such locally generated tsunamis are included in the modeling to provide data for planning. The Nankai and Ryukyu sources belong to the same subduction zone. The former is considered for modeling because of its higher seismicity associated with stronger coupling and larger, preferred maximum magnitude. Tsunamigenic earthquakes at Nankai Trough have recurrence intervals of 100 to 200 years during the last 1300 years (Ando, 1975). The presence of comprehensive records and measurements explains the narrow parameter ranges in the table. The plate boundary along Philippine Trench represents the source for tsunamis from the west and the large dip angle make it effective in generating uplift. New Guinea and Manus belong to separate subduction zones, but the resulting tsunamis have similar impacts to Guam. The New Guinea subduction zone, which has higher seismicity, is selected as a representative tsunami source from the south.

Table 1. Seismicity of tsunami sources with potential impact to Guam

Tsunami Source		Dip (°)	Convergence Rate (mm/yr)	Coupling Coefficient (Preferred)	Maximum Magnitude (Preferred)
Local	Mariana	22	63	0.1 - 0.7 (0.20)	7.2 - 9.5 (8.3)
North	Nankai	13	50	0.8 - 1.0 (0.90)	8.5 - 8.9 (8.7)
	Ryukyu	17	96	0.1 - 0.7 (0.20)	8.0 - 9.1 (8.5)
West	Philippine	46	36	0.1 - 0.8 (0.25)	7.6 - 9.3 (8.5)
South	New Guinea	8	22	0.6 - 0.8 (0.70)	8.2 - 9.4 (8.8)
	Manus	15	9	0.3 - 0.7 (0.50)	7.5 - 9.5 (8.5)

We model tsunamis from each source over a moment magnitude range to cover advisory to warning-level tsunamis reaching Guam. The discretization from Gica et al. (2008) provides the fault geometries and parameters for the four selected subduction zones. The rupture area is determined from the moment magnitude using the scaling relation of Ye et al. (2016a, b), who analyzed 114 earthquakes of the circum-Pacific mega-thrusts with Mw ≥ 7.0 from 1990 to 2015. The proposed width to length ratio of 0.2423 allows determination of the fault dimensions in the dip and strike directions. The rupture within each zone is aligned with the trench and positioned to give the most direct path of the resulting tsunamis to Guam as illustrated in Figure 2. When the rupture reaches the full width of the subduction zone, we extend the fault length to match the rupture area associated with the seismic moment. A typical value of 3×10^{10} N/m^2, consistent with Ye et al. (2016a, b), accounts for the rigidity in the computation of the average slip using the scaling relation of Kanamori (1997).

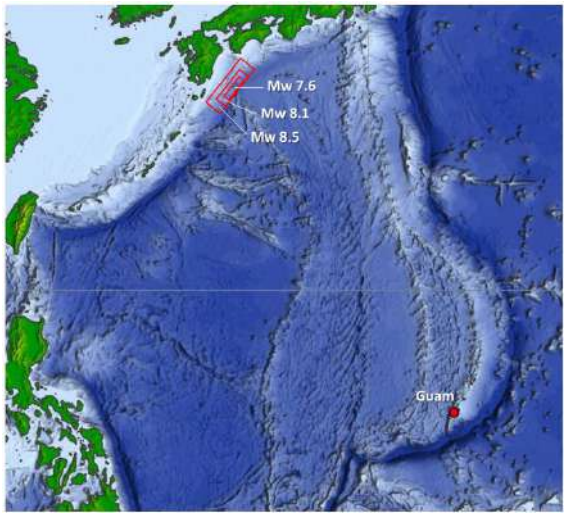

Figure 2. Illustration of rupture models at Nankai Trough.

Table 2. Source parameters as functions of earthquake magnitude

Mw	Area (km^2)	Length (km)	Width (km)	Up-dip slip (m)	Down-dip slip (m)
7.5	2239	96	23	4.2	2.1
7.6	2818	108	26	4.7	2.3
7.7	3548	121	29	5.3	2.6
7.8	4467	136	33	5.9	3.0
7.9	5623	152	37	6.7	3.3
8.0	7080	171	41	7.5	3.7
8.1	8912	192	46	8.4	4.2
8.2	11220	215	52	9.4	4.7
8.3	14125	241	58	10.5	5.3
8.4	17783	271	66	11.8	5.9
8.5	22387	300	75	13.3	6.6
8.6	28184	341	83	14.9	7.4
8.7	35481	383	93	16.7	8.3
8.8	44649	446	100	18.7	9.4

While the scaling relation of Kanamori (1977) provides the average slip for a given moment magnitude, recent tsunami hazard assessments for California and Hawaii have placed larger slip toward the trench to mimic the rupture of the 2011 Tohoku earthquake (e.g., Ross et al., 2013; Bai et al., 2018). Following the approach of Bai et al. (2018), we place twice the slip in the up-dip half of the rupture area to produce more energetic tsunamis for the same seismic moment. Table 2 lists the seismic source parameters as functions of moment magnitude for the earthquake scenarios at the Mariana, Nankai, Philippine, and New Guinea subduction zones. Although the source parameters only depend on the moment magnitude, the resulting tsunami is also influenced by the local tectonics and water depth.

2. Model Setup

We utilize NEOWAVE to model each tsunami from its source to Apra Harbor. The staggered finite-difference model builds on the nonlinear shallow-water equations with a vertical velocity term to account for dispersive tsunami waves and a momentum conservation scheme to describe flow discontinuities (Yamazaki et al., 2009, 2011). These specialized features enable modeling of the vertical flow structure over steep volcanic slopes as well as tsunami bores and hydraulic jumps that might develop in the shallow-reef environment of the Mariana Islands. NEOWAVE has been validated with laboratory and field benchmarks for modeling of coastal currents and inundation by the National Tsunami Hazard Mitigation Program (Yamazaki et al., 2012; Bai et al., 2015).

Modeling of tsunami propagation and inundation requires a digital elevation model of increasing resolution from the open ocean to the coast. We utilize the General Bathymetry Chart of the Oceans (GEBCO) at 30 arcsec (~900 m) resolution for the open ocean and a blended, high-resolution dataset near Guam consisting of

- 2001 USACE SHOALS LiDAR bathymetry to 40 m depth at 4 m resolution
- 2003 University of Hawaii SOEST multibeam bathymetry to 3.5 km depth at 60 m resolution

- 2007 University of Hawaii SOEST multibeam bathymetry to 400 m depth at 5 m resolution
- 2007 USACE LiDAR topography at 0.5 m resolution for the entire island of Guam
- 2007 USACE LiDAR bathymetry at 4 m resolution (limited coverage)
- 2008 US Navy & NOAA multibeam bathymetry of Apra Harbor at 1 m resolution

The dataset is supplemented by digitization of NOAA Chart Nos. 4196 and 4197 at shallow reefs, aerial images from Google Earth, and information gathered during the field visit from January 15 to 19, 2018. We use the *bare-earth* data, which excludes buildings and vegetation, in the digital elevation model to be consistent with the standard practice for tsunami inundation mapping.

Four levels of telescopic grids in spherical coordinates are needed to model the tsunami from each earthquake source with increasing resolution to Apra Harbor. Figure 3 shows the layout of the computational grid systems. The grid nesting scheme includes two-way communications during the computation and does not require external transfer of data between grid layers. Each grid contains bathymetric features of a scale appropriate to the resolution and physical processes. A level-1 grid at 2-arcmin (~3700 m) resolution describes tsunami propagation from the Nankai source to Guam and a second level-1 grid, shifted to the south, caters to the Mariana, Philippine, and New Guinea sources. The level-2 grid captures wave transformation along the Mariana Island chain at higher resolution of 24 arcsec (~720 m) and provides a transition to the 3-arcsec (~90 m) level-3 grid that can resolve the steep slopes and narrow shelves around Guam. The level-4 grid covers Apra Harbor and the adjacent areas. The 0.3 arcsec (~9 m) resolution provides an accurate description of the nearshore reef systems and waterways for computation of currents and inundation at the shore.

Pile-supported docks and piers, which allow passage of the flow underneath, are often represented as terrain features in LiDAR topography. These structures were removed from the level-4 computational grid, if their presence is expected to modify the surrounding flow in a substantial way, and the elevation between the bulkhead and dockside was interpolated. A Manning coefficient of 0.035 describes the subgrid roughness of tropical island environments (Bretschneider et al., 1986), while a value of 0.025 is optimal in resolving currents in harbors (Bai et al., 2015). The Mean Higher High Water (MHHW) and the Mean Lower Low Water (MLLW) levels at the Apra Harbor tide gauge are 0.296 and 0.419 m above and below the mean sea level (MSL) (https://tidesandcurrents.noaa.gov). The 0.715-m tide range is unlikely to have appreciable effects on the tsunami flow in Apra Harbor. Unless noted otherwise, the MSL is used to represent an average conditions in the development of the data products.

3. Data Products

The computation covers 5 hours of elapsed time after arrival of each tsunami at Apra Harbor. This allows development of multi-scale standing waves in the harbor basins, over the Guam insular slopes, and along the Mariana Islands that together contribute to strong surges and currents commonly observed in tropical island environments after a tsunami (Roeber et al., 2010; Cheung et al., 2013). NEOWAVE produces a large volume of spatial and temporal data at various coverage and resolution for post-processing. This section provides samples of the data products for illustration.

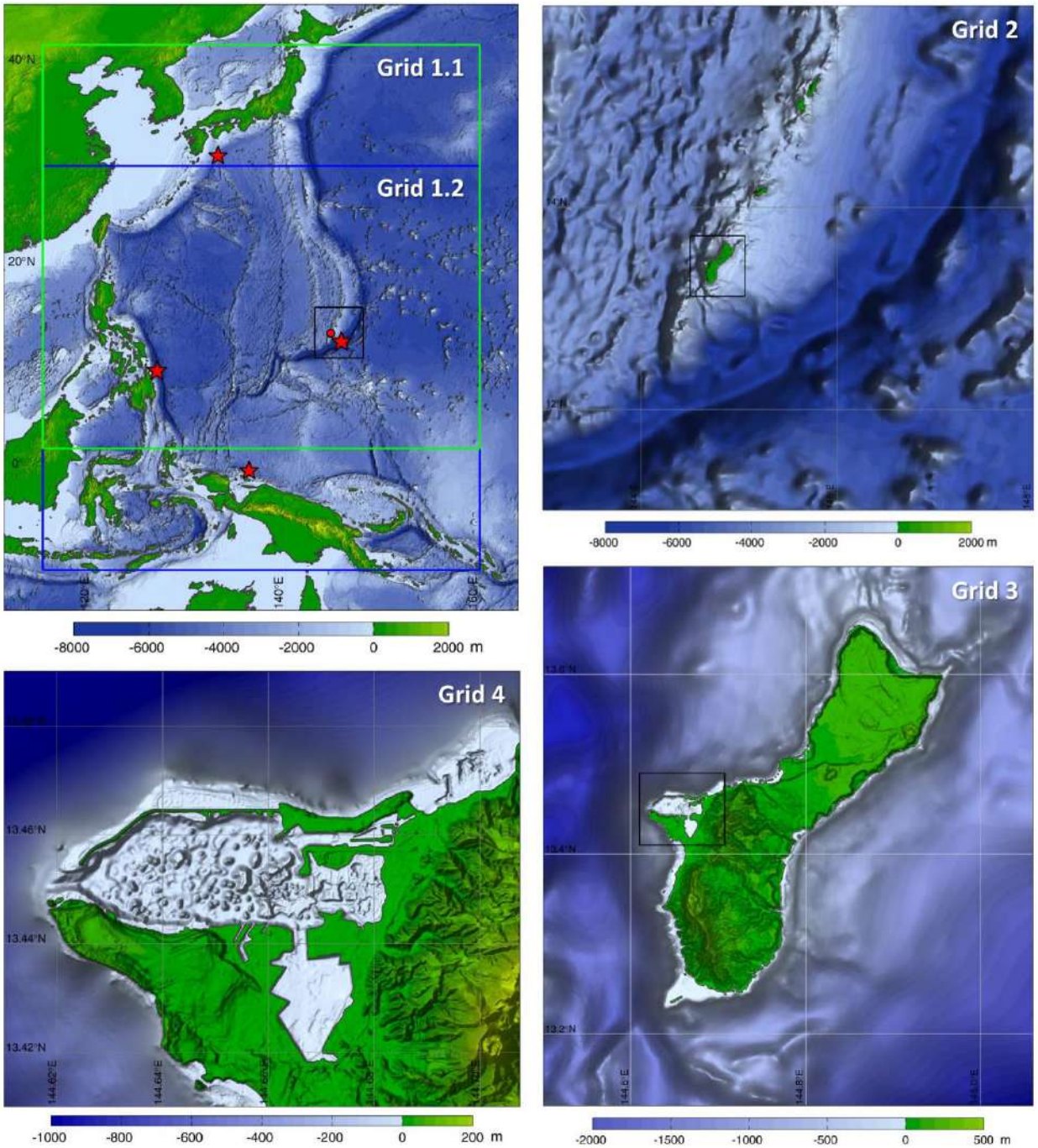

Figure 3. Layout of computational grids. Red circle and stars denote locations of Apra Harbor and tsunami sources.

3.1 Advisory-level Scenarios

The Mariana source is located immediately to the southeast of Guam and a tsunami generated there takes 6 min to reach the entrance of Apra Harbor. Figure 4 shows the surge, drawdown, and current from tsunamis generated by *Mw* 7.6, 7.8, and 8.0 earthquakes. The three events illustrate the data products in terms of the earthquake magnitude and potential impact. The *Mw* 7.6 event, which

produces nearshore wave amplitude of less than 1 m, is at the advisory level for Apra Harbor. The *Mw* 7.8 event is at the threshold for inundation, while the *Mw* 8.0 is well above the warning level with potential inundation on open coasts. There is a notable decrease of wave action in the outer basin due to the narrow entrance from the ocean and the large body of sheltered water as deep as 50 m. The 1993 *Mw* 7.8 Guam earthquake produced a tsunami with reported inundation at the low-lying shore of Sasa Bay, but only 0.15 m amplitude recorded at the tide gauge near the entrance to Sumay Cove Marina (Lander et al., 2002). The corresponding surge of 0.19 m from the *Mw* 7.8 scenario corroborates the tide gauge measurement. The model results show an overall increase of wave action from the center of the basins to the shores especially at the commercial harbor, where the surge and drawdown reach 0.55 m for the threshold event. Local speed-up of the current is evident over the shallow reefs including Piti Channel east of the commercial harbor.

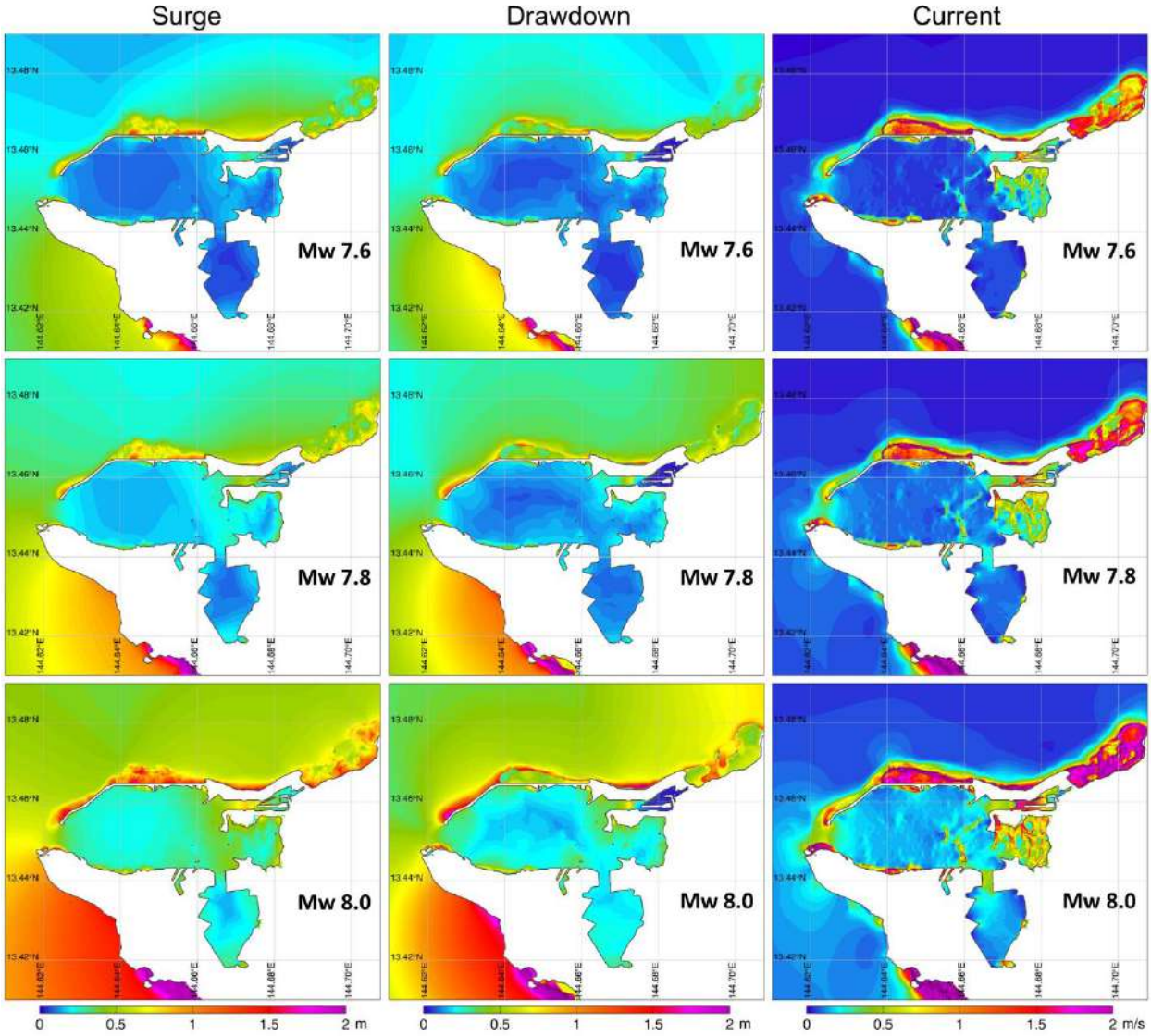

Figure 4. Surge, drawdown, and current at Apra Harbor from the *Mw* 7.6, 7.8, and 8.0 Mariana Trench earthquake scenarios.

The Nankai subduction zone is located 2300 km from Guam with a tsunami travel time of 3 hours. Damaging tsunamis to Apra Harbor would involve larger earthquakes at the distant source. Figure 5 shows the surge, drawdown, and current from tsunamis generated by *Mw* 8.3, 8.5, and 8.7 earthquakes. The selected events demonstrate the impact as the surge transitions from advisory to warning levels. The longer waves associated with the larger rupture area produce notable resonance oscillations at Apra Harbor. The surge increases gradually from the entrance to the eastern end of the outer basin and remains rather uniform in the inner basin. The reduced amplitude at both entrances indicates formation of nodes, each of which serves as a conduit between two oscillating bodies of water. The oscillations between the inner and outer basins and the wave motion outside the harbor are connected through the nodes with energy exchange. The low damping of the wave motion over the steep insular slopes alludes to a continuous supply of energy from the open ocean to the oscillations inside the harbor. With the threshold event as an example, the pumping motion between the outer and inner basins creates a strong current of 2.5 m/s at the inner channel versus a value of 1.4 m/s at the main entrance.

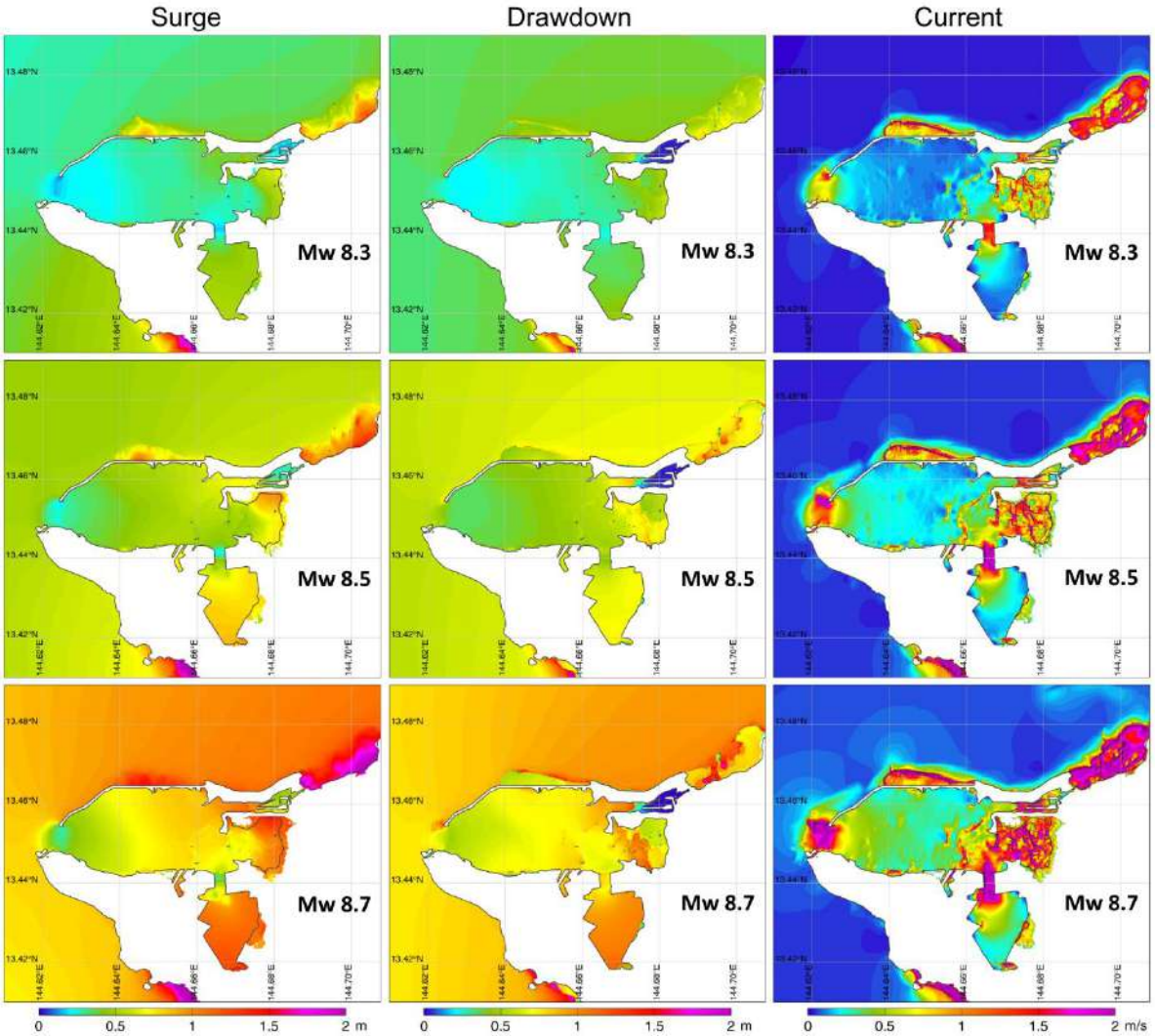

Figure 5. Surge, drawdown, and current at Apra Harbor from the *Mw* 8.3, 8.5, and 8.7 Nankai Trough earthquake scenarios.

Tsunamis from the Philippine source have the most direct approach to Apra Harbor. The travel time of 2.5 hr is shorter compared to Nankai trough events due to the slightly shorter distance of 2000 km and deeper water in the East Philippine Sea. The deep water at the trench enhances the energy of the tsunami generated by seafloor deformation while reducing the wave period. Figure 6 shows the transition from advisory to warning-level tsunamis generated by *Mw* 8.1, 8.3, and 8.5 earthquakes. The response pattern is similar to those generated by local events with a single node at the channel between the inner and outer basins. This means the oscillations in the harbor is not fully coupled with the standing edge waves on the steep insular slopes. Strong currents reaching 1.0 and 2.2 m/s for the threshold *Mw* 8.3 event do occur at the entrances to the outer and inner basins, while the surge reaches 0.74 and 0.79 m at the commercial harbor and the south end of the inner basin.

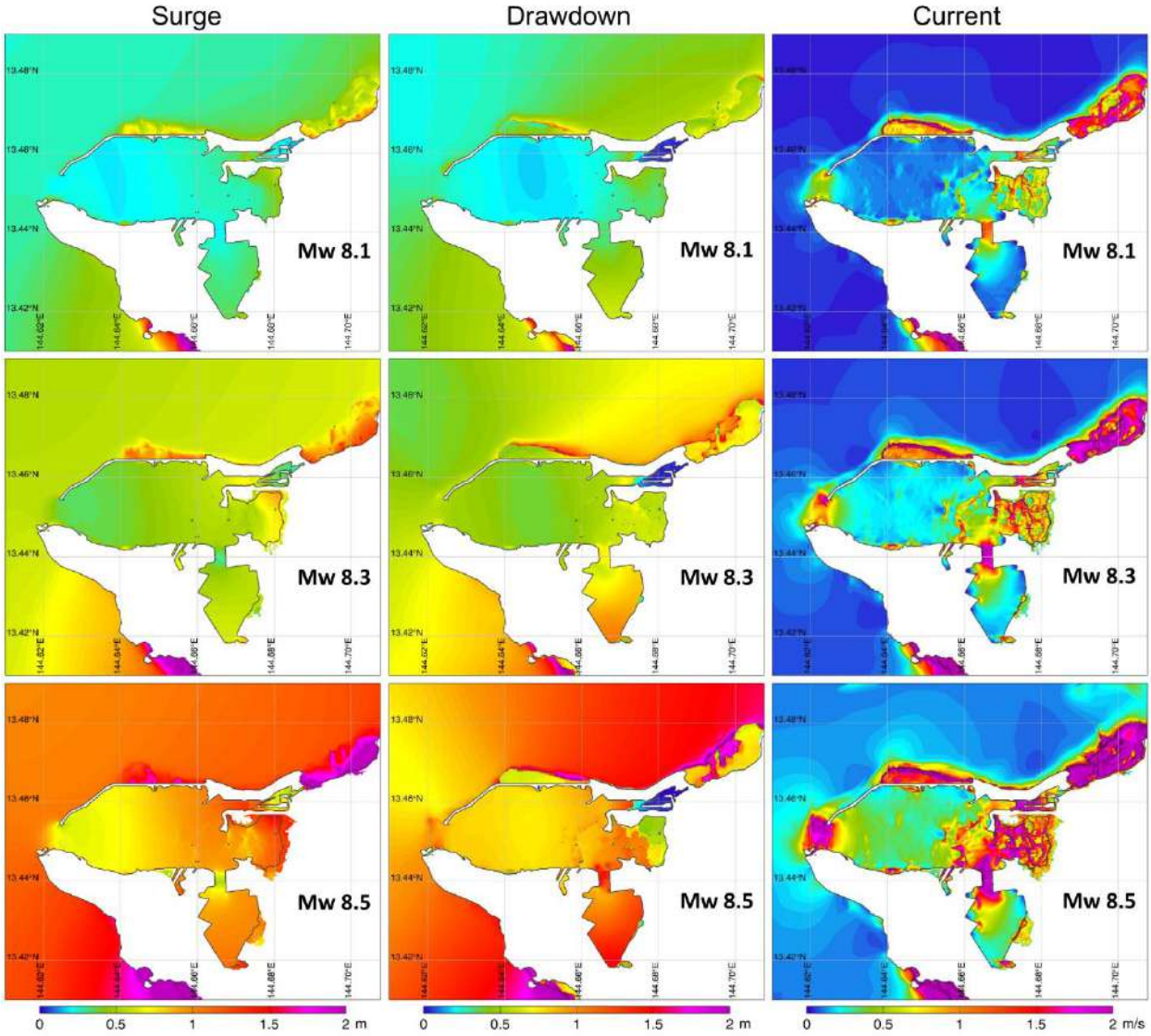

Figure 6. Surge, drawdown, and current at Apra Harbor from the *Mw* 8.1, 8.3, and 8.5 Philippine Trench earthquake scenarios.

The New Guinea subduction zone is 1800 km from Guam with a travel time of 2.4 hr. The small dip angle of the fault plane is ineffective in generating seafloor uplift from earthquake rupture. The resulting tsunamis reaching Guam also have their amplitude reduced by diversion of the energy through Yap Trench and Mariana Trench. Any significant tsunami events from the New Guinea source will involve large earthquake magnitude. Figure 7 shows the transition from advisory to warning-level tsunamis generated by *Mw* 8.4, 8.6, and 8.8 earthquakes. The oscillation pattern is similar to those from the Philippine source with one distinct node at the channel between the outer and inner basins. The surge reaches 0.52 and 0.61 m at the commercial harbor and the southern end of the inner basin, while the current reaches 1.3 m/s at the entrance channel to the inner basin for the *Mw* 8.6 threshold event.

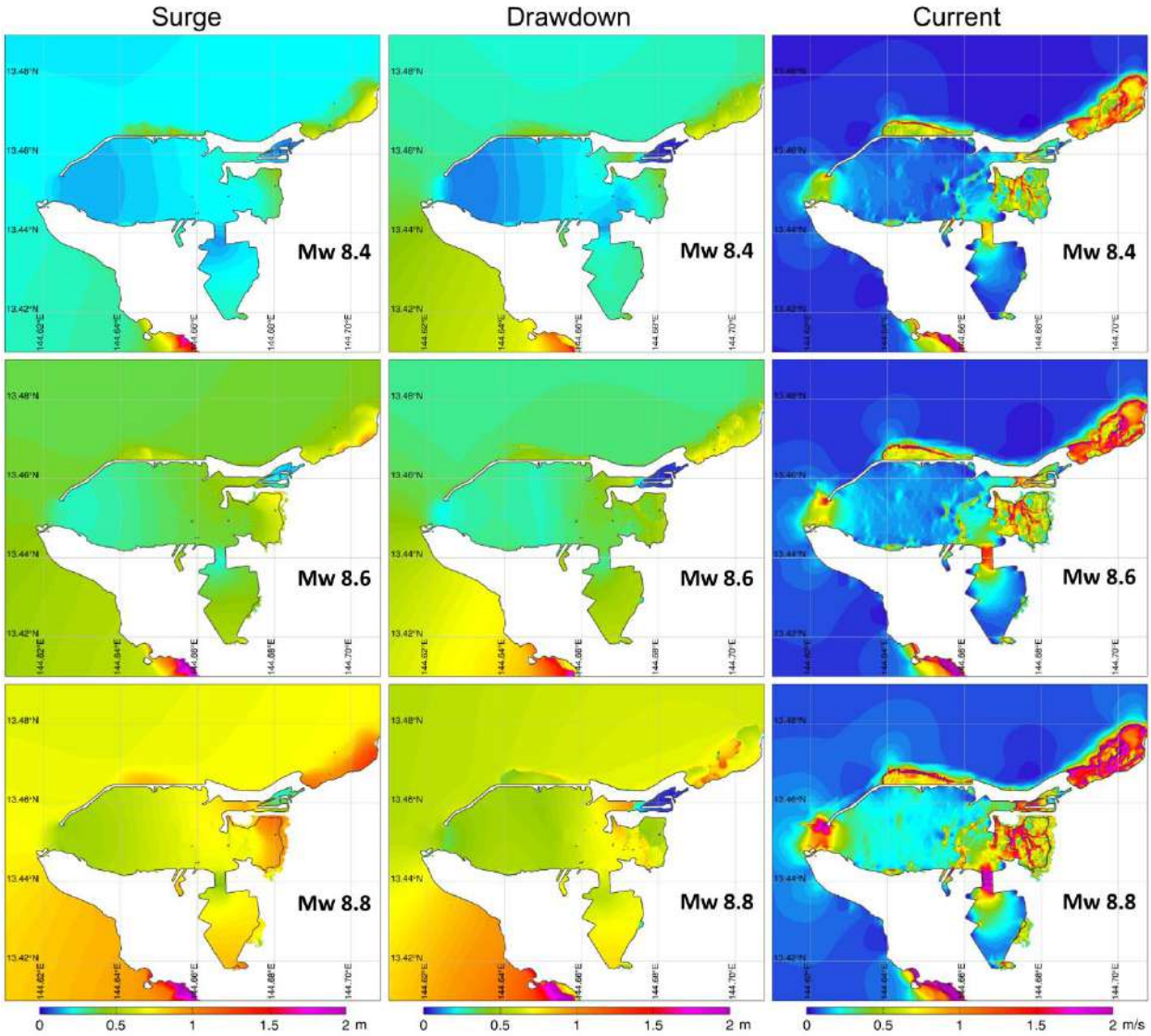

Figure 7. Surge, drawdown, and current at Apra Harbor from the *Mw* 8.4, 8.6, and 8.8 New Guinea earthquake scenarios.

3.2 Probable Maximum Scenarios

The USCG District 14 emergency response plan calls for evacuation of vessels from ports and harbors for all warning-level tsunamis. The preferred maximum earthquakes from Berryman et al. (2015) at the four most critical subduction zones to Guam can provide credible worse-case scenarios to determine where vessels need to be evacuated to. However, it is necessary to consider locally-generated and far-field tsunamis separately in the response plan due to their distinct characteristics.

Figure 8 shows the surge, drawdown, and current for the preferred, maximum Mariana scenario with *Mw* 8.3. The local tsunami severely impacts the east and north-facing shores of Guam. The waves arrive at the harbor entrance 6 min after the earthquake and reach maximum amplitude inside the harbor 9 min afterward. The short timeframe precludes any warning instructions from being implemented and might be insufficient for vessels to get underway. A strong earthquake will be a sign of an imminent tsunami. Apra Harbor provides a very good shelter from local tsunamis. With less than 0.5 m of surge and drawdown and 0.4 m/s of current, the central portion of the outer basin appears to be viable as a refuge for evacuated vessels. In comparison, the surge/drawdown and current reach 1.5 m and 1.0 m/s at the Port of Guam. The entrances to the outer and inner basins show moderate increase of the current to 1.2 and 1.6 m/s.

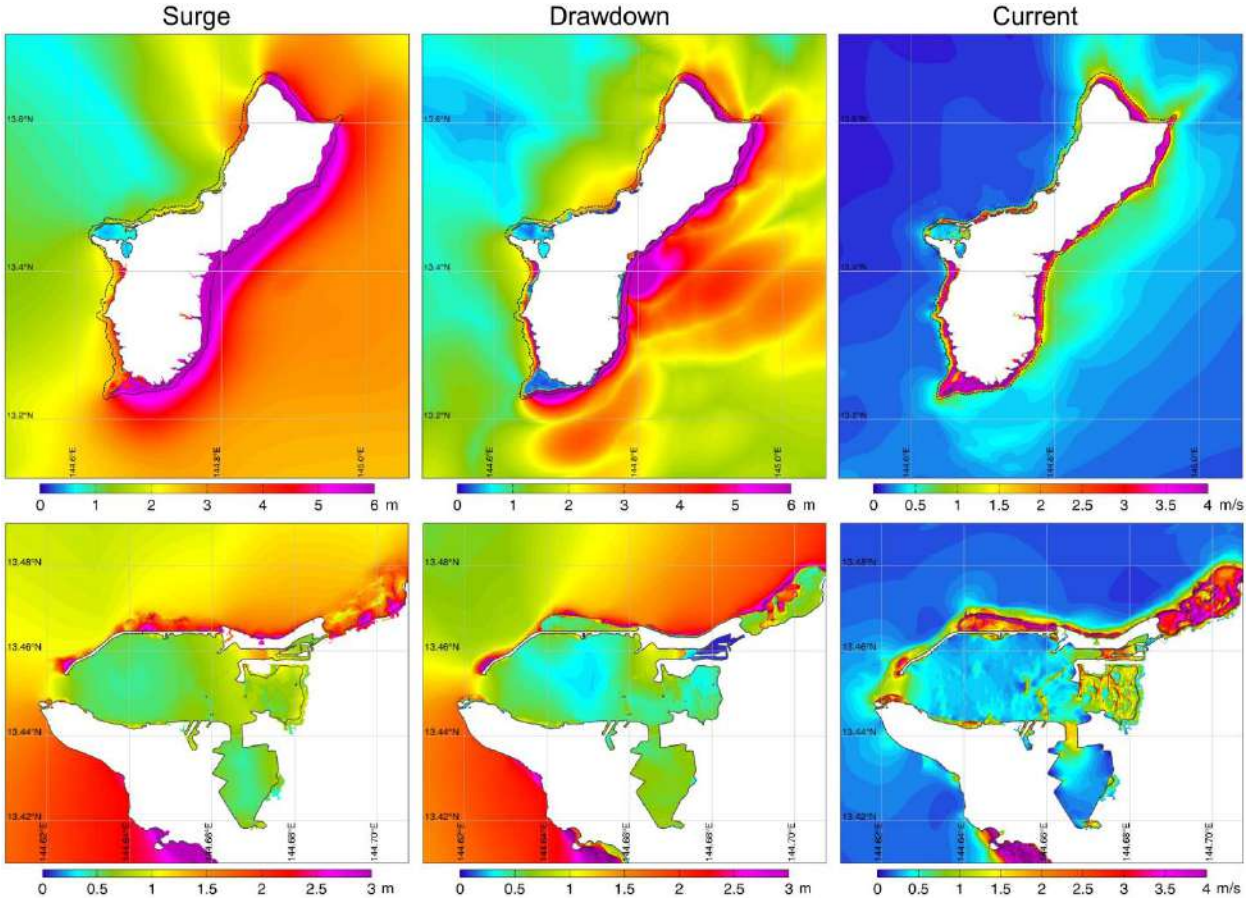

Figure 8. Surge, drawdown, and current from tsunamis generated by the preferred maximum earthquake at Mariana Trench. Black solid lines denote the coastlines, and in the upper panels, the black dash lines indicate the 100-m depth contour delineating the approximate extent of the insular shelf.

A tsunami from the Nankai, Philippine, and New Guinea sources has at least 2.4 hours of travel time to the entrance of Apra Harbor. If a tsunami warning is issued in time, most of the vessels might be able to evacuate from their docks to designated areas with reduced wave action. Among the three probable maximum far-field tsunamis, the *Mw* 8.5 Philippine scenario has the most severe impact overall. The results are aggregated with those from the *Mw* 8.7 Nankai and 8.8 New Guinea scenarios to account for localized responses due to directivity and resonance of the tsunamis. Figure 9 shows the aggregated surge, drawdown, and current. Apra Harbor remains a good shelter from far-field tsunamis despite notable amplification over the insular slopes especially off the north-facing shores. The central portion of the outer basin, which has less than 0.8 m of surge and drawdown and 0.4 m/s of current, can serve as a refuge for evacuated vessels. The conditions are far more favorable in comparison to those at the 100 m depth contour, which is the upper limit for demarcation of refuge areas by NTHMP partner states and territories. In comparison, the surge/drawdown and current at the Port of Guam reaches 1.4 m and 1.2 m/s due to local amplification. The longer period tsunami waves from the distant sources trigger resonance oscillations in the harbor with currents reaching 2.6 and 4.2 m/s at the outer and inner basin entrances.

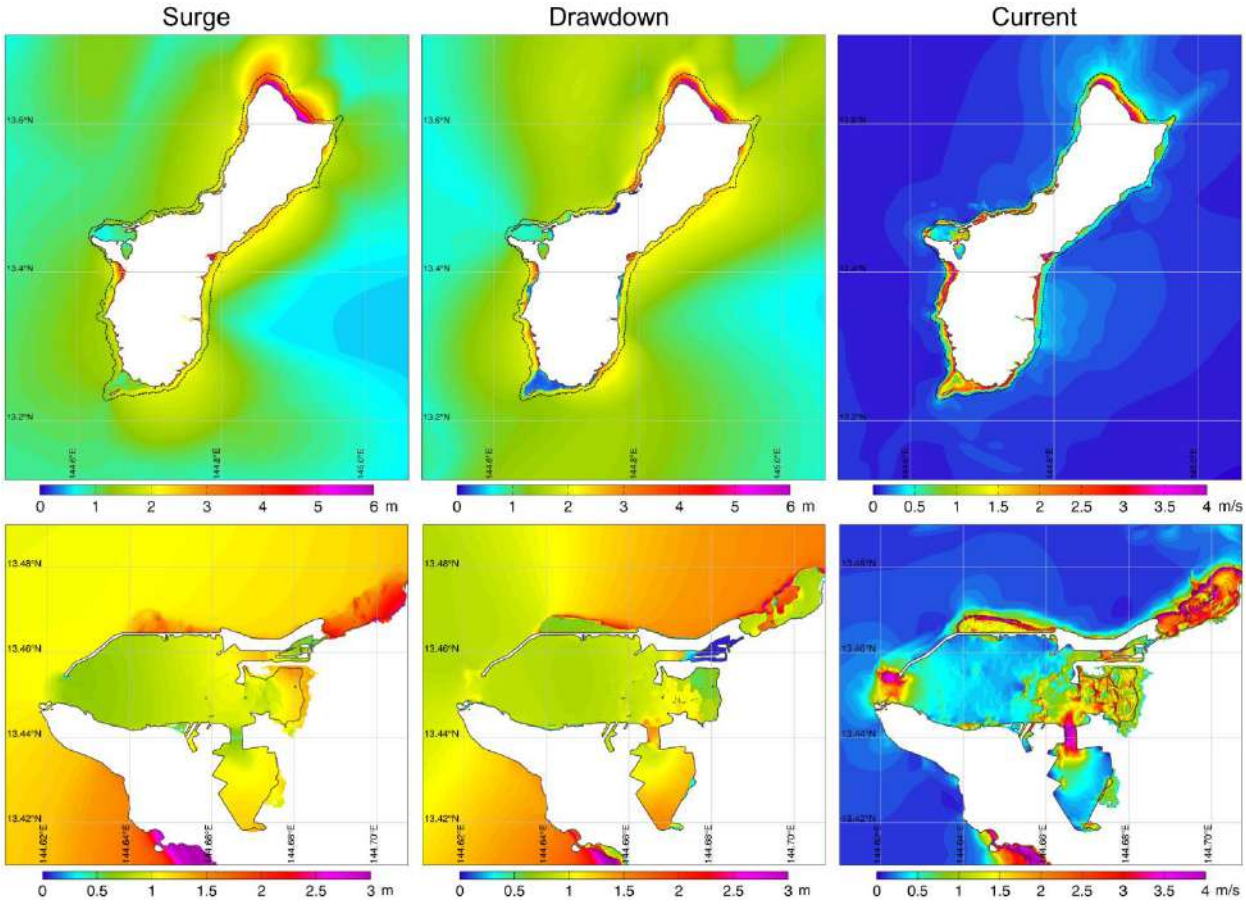

Figure 9. Aggregated surge, drawdown, and current from tsunamis generated by the preferred maximum earthquakes at Philippine Trench, Nankai Trough, and New Guinea Trench. Black solid lines denote the coastlines, and in the upper panels, the black dash lines indicate the 100-m depth contour delineating the approximate extent of the insular shelf.

4. Summary Tables

The modeling work has produced a large volume of spatial data for the surge, drawdown, and current at Apra Harbor from tsunamis generated by potential Mariana, Nankai, Philippine, and New Guinea earthquakes. These scenarios cover a range of earthquake magnitude up to the preferred maximum suggested by Berry et al. (2015). Apra Harbor encompasses a large area with scattered facilities under multiple jurisdictions. We delineated four critical areas in consultation with USCG Guam Sector. These are the main entrance, Kilo Wharf, Port of Guam, and the inner basin entrance as shown in Figure 10. Summary tables of potential impacts in these areas allow quick assessment of the situation and formulation of a course of action during the initial stage of a tsunami.

Tables 3 through 6 list the maximum surge, drawdown, and current in the four critical areas as functions of earthquake magnitude for the Mariana, Nankai, Philippine, and New Guinea sources. The modeling work is based on the mean-sea level such that the tabulated surge and drawdown will reference the tide level during an actual event. The dynamic response is multi-modal due to broad-band excitation of the oscillation modes tied to the harbor configuration. The tables also include periods of the two most energetic oscillation components in each area. There is a general upward trend of the surge, drawdown, current, and the respective oscillation periods with earthquake magnitude. The variation, however, is not continuous due to transition from one oscillation mode to another as the excitation periods increase for larger earthquakes. This is most evident in the abrupt increases of the oscillation period or the energy level of one component versus the other at specific earthquake magnitudes. As the maximum surface elevation and current are driven by distinct oscillation modes at separate locations within each area of interest, their dominant periods are typically different.

Figure 10. Critical areas at Apra Harbor for compilation of summary tables.

Table 3. Maximum surge, drawdown, and current at Apra Harbor from Mariana Trench tsunamis

Mariana Mw	Main Entrance				
	Surge (ft)	Drawdown (ft)	Period (min)	Current (knots)	Period (min)
7.7	1.2	1.6	10, 15	1.3	19, 43
7.8	1.6	1.8	10, 12	1.5	43, 19
7.9	2.3	2.7	10, 12	1.8	43, 19
8.0	3.0	4.1	10, 12	2.1	43, 19
8.1	3.6	4.8	10, 12	2.2	43, 22
8.2	4.4	5.9	10, 12	3.9	43, 22
8.3	4.9	6.1	10, 12	4.5	43, 22
	Kilo Wharf				
	Surge (ft)	Drawdown (ft)	Period (min)	Current (knots)	Period (min)
7.7	0.5	0.5	8, 19	0.3	10, 19
7.8	0.6	0.5	8, 19	0.3	10, 43
7.9	0.8	0.7	8, 19	0.4	10, 43
8.0	1.0	1.0	8, 19	0.5	43, 10
8.1	1.2	1.1	8, 22	0.7	43, 10
8.2	1.5	1.4	8, 22	0.9	43, 22
8.3	1.8	2.0	8, 42	1.1	43, 22
	Port of Guam				
	Surge (ft)	Drawdown (ft)	Period (min)	Current (knots)	Period (min)
7.7	1.6	1.5	9, 19	0.8	8, 6
7.8	2.0	2.0	9, 19	0.9	8, 6
7.9	2.7	2.1	9, 19	1.1	8, 6
8.0	2.9	2.6	10, 43	1.2	8, 10
8.1	3.3	2.4	10, 43	1.4	8, 10
8.2	4.0	3.3	10, 43	1.7	10, 22
8.3	4.9	4.5	10, 43	2.4	10, 40
	Inner Basin Entrance				
	Surge (ft)	Drawdown (ft)	Period (min)	Current (knots)	Period (min)
7.7	0.8	0.6	9, 42	0.4	24, 42
7.8	1.0	0.8	9, 42	0.7	24, 43
7.9	1.2	1.0	10, 43	0.9	23, 43
8.0	1.5	1.0	10, 43	1.2	23, 43
8.1	1.8	1.2	43, 10	1.7	22, 43
8.2	2.3	1.5	43, 10	2.3	22, 43
8.3	3.0	2.2	43, 8	3.5	43, 22

The Mariana tsunamis trend to have short periods that do not fully excite the resonance modes of Apra Harbor. The surge, drawdown, and current, which are maximum at the main entrance, rapidly attenuate to less than one third of the values at Kilo Wharf a short distance away. Localized oscillations along with shoaling bring a mild increase of the impacts at the Port of Guam. Resonance oscillations between the inner and outer basins begin to develop at *Mw* 8.3 as indicated by the abrupt increase of the current at the channel between the two basins.

Table 4. Maximum surge, drawdown, and current at Apra Harbor from Nankai Trough tsunamis

Nankai Mw	Main Entrance				
	Surge (ft)	Drawdown (ft)	Period (min)	Current (knots)	Period (min)
8.1	0.6	1.0	24, 15	2.6	18, 24
8.2	0.8	1.2	24, 15	3.2	18, 24
8.3	0.9	1.6	24, 17	4.3	18, 24
8.4	1.1	2.3	24, 17	5.1	17, 24
8.5	1.3	3.1	24, 17	5.5	17, 24
8.6	1.8	3.6	24, 17	6.7	17, 24
8.7	2.4	4.3	24, 17	8.0	17, 46
	Kilo Wharf				
	Surge (ft)	Drawdown (ft)	Period (min)	Current (knots)	Period (min)
8.1	0.4	0.5	24, 18	0.3	18, 24
8.2	0.6	0.6	24, 18	0.3	18, 24
8.3	0.8	0.8	24, 18	0.4	17, 24
8.4	1.0	1.0	24, 18	0.6	17, 24
8.5	1.2	1.2	24, 50	0.8	17, 40
8.6	1.5	1.5	24, 50	1.1	17, 51
8.7	1.8	2.0	23, 51	1.4	17, 51
	Port of Guam				
	Surge (ft)	Drawdown (ft)	Period (min)	Current (knots)	Period (min)
8.1	1.1	1.6	18, 24	0.5	18, 24
8.2	1.3	1.8	24, 17	0.6	18, 24
8.3	1.6	2.0	24, 17	0.7	17, 24
8.4	2.0	2.4	24, 17	0.8	17, 24
8.5	2.5	3.1	24, 17	1.0	17, 23
8.6	3.3	3.9	24, 17	1.1	17, 23
8.7	3.8	4.6	23, 19	2.0	17, 27
	Inner Basin Entrance				
	Surge (ft)	Drawdown (ft)	Period (min)	Current (knots)	Period (min)
8.1	1.0	0.7	24, 40	2.3	24, 28
8.2	1.1	0.9	24, 40	3.2	24, 28
8.3	1.5	1.2	24, 40	4.1	24, 28
8.4	2.0	1.7	24, 40	5.2	24, 28
8.5	2.6	2.4	24, 40	6.9	24, 28
8.6	3.1	3.4	24, 40	7.2	24, 40
8.7	3.6	4.8	23, 46	7.5	23, 40

Tsunamis from the three far-field sources have longer oscillation periods that can excite coupled oscillations between the harbor basins and island-trapped waves. The relatively small surface elevations and strong currents indicate formation of nodes at the two entrances, which should be avoided during both local and far-field tsunamis. There is slight amplification of the surge and

Table 5. Maximum surge, drawdown, and current Apra Harbor from Philippine Trench tsunamis

Philippine Mw	Main Entrance				
	Surge (ft)	Drawdown (ft)	Period (min)	Current (Knots)	Period (min)
7.9	0.7	0.6	9, 20	1.0	43, 23
8.0	0.8	0.8	9, 23	1.4	43, 23
8.1	1.0	1.1	9, 32	2.0	43, 23
8.2	1.3	1.6	9, 32	3.8	43, 23
8.3	1.7	2.0	9, 32	4.5	43, 23
8.4	2.4	2.8	9, 32	6.5	43, 22
8.5	3.2	3.7	9, 32	7.3	43, 22
	Kilo Wharf				
	Surge (ft)	Drawdown (ft)	Period (min)	Current (knots)	Period (min)
7.9	0.5	0.4	23, 43	0.2	43, 23
8.0	0.6	0.6	23, 43	0.3	43, 23
8.1	0.8	0.8	23, 43	0.4	43, 23
8.2	1.0	1.1	23, 43	0.5	43, 22
8.3	1.3	1.5	23, 43	0.6	43, 22
8.4	1.6	2.1	23, 43	0.9	43, 22
8.5	2.2	2.8	47, 23	1.2	43, 22
	Port of Guam				
	Surge (ft)	Drawdown (ft)	Period (min)	Speed (knots)	Period (min)
7.9	0.7	0.7	43, 23	0.3	9, 23
8.0	1.0	1.0	43, 23	0.5	9, 22
8.1	1.5	1.4	43, 23	0.7	9, 23
8.2	1.8	1.9	22, 43	0.9	9, 22
8.3	2.5	2.5	43, 23	1.3	9, 22
8.4	3.2	3.1	43, 22	1.7	9, 22
8.5	4.3	4.1	43, 22	2.2	9, 22
	Inner Basin Entrance				
	Surge (m)	Drawdown (m)	Period (min)	Speed (m/s)	Period (min)
7.9	0.6	0.7	43, 23	1.3	23, 43
8.0	0.9	1.0	43, 21	1.9	23, 43
8.1	1.0	1.4	43, 23	2.6	23, 43
8.2	1.5	1.9	43, 22	3.5	23, 43
8.3	1.8	2.6	43, 22	4.9	23, 43
8.4	2.4	3.3	43, 22	6.0	22, 32
8.5	3.2	5.3	43, 22	8.2	22, 32

drawdown in the port area, but the current remains moderate even for large events. Similar to the local tsunamis, Kilo Wharf is relatively calm despite its proximity to the main entrance. The relatively deep, outer basin serves as a buffer for attenuation of the tsunami waves passing through the narrow entrance channel.

Table 6. Maximum surge, drawdown, and current at Apra Harbor from New Guinea Trench tsunamis

New Guinea Mw	Main Entrance				
	Surge (ft)	Drawdown (ft)	Period (min)	Current (knots)	Period (min)
8.2	0.4	0.7	11, 20	1.9	22, 43
8.3	0.5	0.9	11, 20	2.4	22, 46
8.4	0.7	1.0	11, 28	2.8	24, 46
8.5	0.9	1.2	11, 28	3.3	46, 22
8.6	1.2	1.3	17, 28	3.8	46, 24
8.7	1.6	1.9	17, 27	4.8	46, 23
8.8	2.1	2.1	17, 27	5.4	46, 23
	Kilo Wharf				
	Surge (ft)	Drawdown (ft)	Period (min)	Current (knots)	Period (min)
8.2	0.3	0.2	24, 20	0.2	43, 23
8.3	0.4	0.3	22, 20	0.3	43, 23
8.4	0.5	0.4	24, 43	0.3	43, 23
8.5	0.7	0.7	22, 43	0.4	43, 22
8.6	0.9	1.0	43, 24	0.5	43, 17
8.7	1.2	1.3	43, 22	0.7	43, 17
8.8	1.6	1.6	43, 26	0.8	43, 17
	Port of Guam				
	Surge (ft)	Drawdown (ft)	Period (min)	Current (knots)	Period (min)
8.2	0.5	0.9	23, 43	0.2	11, 23
8.3	0.7	1.2	22, 46	0.3	11, 23
8.4	1.0	1.4	24, 43	0.4	24, 11
8.5	1.3	1.5	43, 22	0.5	22, 46
8.6	1.7	1.8	43, 23	0.5	17, 43
8.7	2.3	2.3	43, 23	0.6	17, 43
8.8	3.0	3.1	43, 23	0.8	17, 43
	Inner Basin Entrance				
	Surge (m)	Drawdown (m)	Period (min)	Current (m/s)	Period (min)
8.2	0.4	0.5	24, 43	1.0	22, 30
8.3	0.5	0.7	24, 43	1.5	22, 30
8.4	0.7	1.0	24, 43	2.0	24, 43
8.5	1.0	1.1	43, 22	2.3	24, 43
8.6	1.3	1.6	43, 23	3.3	24, 43
8.7	1.8	2.1	43, 23	3.8	24, 43
8.8	2.4	2.6	43, 26	4.9	26, 43

Appendix A. Power Plant

At the request of Guam Power Authority, we extended the modeling work to assess the vulnerability of its power plant at Apra Harbor. The scenario is based on a Nankai earthquake at the preferred maximum magnitude of 8.7 according to Berrymore et al. (2015). The resulting tsunami is not the most severe among the four preferred maximum scenarios, but has the highest

probability of occurrence in the near future due to its 100 to 200-year recurrence intervals and the last event being in 1946 (Ando, 1975). The use of the MHHW level for modeling is consistent with NTHMP guidelines and general practice for tsunami inundation mapping.

Figure A1 shows the computed surge and current around the power plant. The results indicate notable surge buildup at the west end of Agana Bay and overtopping of Highway 11 into Piti Channel. The power plant facilities are flooded to an elevation of 2.6 m above MSL. The flow depth and current reach 0.8 m and 1.8 m/s with potential damage to the facilities. The floodwater overtops the southwest side of the fuel containment berm, but this might be an artifact resulting from insufficient resolution of the narrow structure. The power plant's location between Piti Channel and Agana Bay make it vulnerable to tsunami impacts.

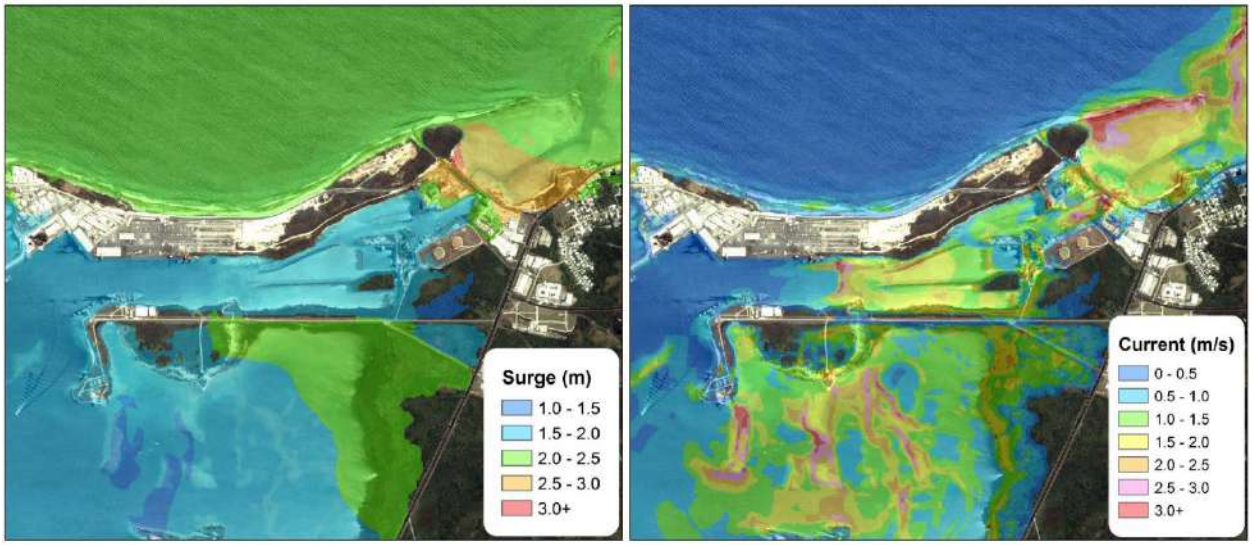

Figure A1. Surge and current at the Port of Guam from the Mw 8.7 Nankai tsunami scenario at high tides.

References

Ando, M. (1975). Source mechanisms and tectonic significance of historical earthquakes along the Nankai Trough, Japan. *Tectonophysics*, 27(2), 119–140.

Bai, Y., Yamazaki, Y., and Cheung, K.F. (2015). NEOWAVE. Proceedings and Results of the 2015 National Tsunami Hazard Mitigation Program Model Benchmarking Workshop, Portland, Oregon, 165-177.

Bai, Y. Yamazaki, Y., and Cheung, K.F. (2018). Amplification of tsunami drawdown and runup in the Hawaiian Islands by near-trench slip of mega Aleutian earthquakes. *Ocean Modelling*, 124, 61-74.

Berryman, K., Wallace, L., Hayes, G., Bird, P., Wang, K., Basili, R., Lay, T., Pagani, M., Stein, R., Sagiya, T., Rubin, C., Barreintos, S., Kreemer, C., Litchfield, N., Stirling, M., Gledhill, K., Costa, C. (2015). The GEM Faulted Earth Subduction Characterization Project, Version 2.0, available from http://www.nexus.globalquakemodel.org/gem-faulted-earth/posts.

Bretschneider, C.L., Krock, H.J., Nakazaki, E., and Casciano, F.M. (1986). Roughness of Typical Hawaiian Terrain for Tsunami Run-up Calculations: A User's Manual. J.K.K. Look Laboratory Report, University of Hawaii, Honolulu, Hawaii.

Cheung, K.F., Bai, Y., and Yamazaki, Y. (2013). Surges around the Hawaiian Islands from the 2011 Tohoku Tsunami. *Journal of Geophysical Research: Oceans*, 118(10), 5703-5719.

Gica, E., Spillane, M.C., Titov, V.V., Chamberlin, C.D., and Newman, J.C. (2008). Development of the Forecast Propagation Database for NOAA's Short Term Inundation Forecast for Tsunamis (SIFT). NOAA Technical Memorandum OAR PMEL-139, Pacific Marine Environmental Laboratory Seattle, WA, 89 pp.

Kanamori, H. (1977). The energy release in great earthquake. *Journal of Geophysical Research*, 82 (20), 2981–2987.

Lander, J.F., Whiteside, L.S., and Hattori, P. (2002). The tsunami history of Guam: 1849-1993. *Science of Tsunami Hazards*, 20(3), 158-174.

Lay, T., Ye, L., Bai, Y., Cheung, K.F., Kanamori, H., Freymueller, J., Steblov, G.M., and Kogan, M.G. (2017). Rupture along 400 km of the Bering Fracture Zone in the Komandorsky Islands Earthquake (Mw 7.8) of 17 July 2017. *Geophysical Research Letters*, 44(24), 12,161–12,169.

Okada, Y. (1985), Surface deformation due to shear and tensile faults in a half space. *Bulletin of the Seismological Society of America*, 75(4), 1135-1154.

Roeber, V., Yamazaki, Y., and Cheung, K.F. (2010). Resonance and impact of the 2009 Samoa tsunami around Tutuila, American Samoa. *Geophysical Research Letters*, 37(21), L21604, Doi: 10.1029/2010GL044419.

Ross, S.L., Jones, L.M., Miller, K, Porter, K.A., Wein, A., Wilson, R.I., Bahng, B., Barberopoulou, A., Borrero, J.C., Brosnan, D.M., Bwarie, J.T., Geist, E.L., Johnson, L.A., Kirby, S.H., Knight, W.R., Long, K., Lynett, P., Mortensen, C.E., Nicolsky, D.J., Perry, S.C., Plumlee, G.S., Real, C.R., Ryan, K., Suleimani, E., Thio, H., Titov, V.V., Whitmore, P.M. and Wood, N.J. (2013). SAFRR (Science Application for Risk Reduction) Tsunami Scenario—Executive Summary and Introduction: U.S. Geological Survey Open-File Report 2013–1170–A, *in* Ross, S.L., and Jones, L.M., eds., The SAFRR (Science Application for Risk Reduction) Tsunami Scenario: U.S. Geological Survey Open-File Report 2013–1170, 17 p., http://pubs.usgs.gov/of/2013/1170/a/.

Yamazaki, Y., Cheung, K.F., and Kowalik, Z. (2011), Depth-integrated, non-hydrostatic model with grid nesting for tsunami generation, propagation, and run-up. *International Journal for Numerical Method in Fluids*, 67(12), 2081-2107.

Yamazaki, Y., K.F. Cheung, Z. Kowalik, G. Pawlak, and T. Lay (2012), NEOWAVE. Proceedings and Results of the 2011 National Tsunami Hazard Mitigation Program Model Benchmarking Workshop, Galveston, Texas, pp. 239-302.

Yamazaki, Y., Kowalik, Z., and Cheung, K.F. (2009). Depth-integrated, non-hydrostatic model for wave breaking and runup. *International Journal for Numerical Method in Fluids*, 61(5), 473-497.

Ye, L., Lay, T., Kanamori, H., and Rivera, L. (2016). Rupture characteristics of major and great ($M_w \geq 7.0$) megathrust earthquakes from 1990 to 2015: 1. Source parameter scaling relationships, *Journal of Geophysical Research: Solid Earth*, 121(2), 826–844.

Ye, L., Lay, T., Kanamori, H., and Rivera, L. (2016). Rupture characteristics of major and great ($M_w \geq 7.0$) megathrust earthquakes from 1990 to 2015: 2. Depth dependence. *Journal of Geophysical Research: Solid Earth*, 121(2), 845–863.